Indian Journal of Pure & Applied Physics
Vol. 63, December 2025, pp. 1170-1180
DOI: 10.56042/ijpap.v63i12.23735

# Adaptive Control of Grid-Connected Solar PV System Under Stochastic Operational Environments

Ram Ishwar Vais[a], Kuldeep Sahay[b] & Tirumalasetty Chiranjeevi[c*]

[a]Department of Electrical Engineering, Rajkiya Engineering College, Sonbhadra 231 206, India

[b]Department of Electrical Engineering, Institute of Engineering and Technology, Lucknow 226 021, India

[c]School of Electrical Engineering, Shri Mata Vaishno Devi University, Katra 182 320, India

*Received: 16th September 2025; accepted: 21st October 2025*

This paper introduces an Adaline-based control approach for a two-stage grid-integrated solar photovoltaic system (SPVS) in stochastic operating conditions. The Adaline algorithm is capable of estimating the fundamental component necessary to determine reference grid currents from harmonically distorted load currents at the point of common coupling. The Adaline algorithm is more adaptable than conventional methods for the fundamental frequency of the system, and it enables the H-bridge voltage source inverter (VSI) to inject precise currents for harmonic correction. Additionally, the H-bridge VSI injects the active power generated by the integrated SPVS at a unity power factor. Moreover, for the optimal gate drive signals, a model predictive controller (MPC) is implemented, which considers the nonlinear switching dynamics of the H-bridge VSI and the DC-DC converter of the SPVS. To assess the Adaline-based MPC approach in stochastic operating conditions, the two-stage grid-integrated SPVS is developed, and its operation is simulated in MATLAB/Simulink. The results obtained from MATLAB/Simulink and the real-time simulator (OP4512) in both grid- supplying and grid-injecting modes with source and load variations. Also, the observed total harmonic distortion of source current has been improved to align with the IEEE 1547-2018 standard.

**Keywords:** Adaline estimator, Data-driven, Energy mix, Fundamental extraction, Grid-integration, Predictive control, Power quality, Solar power, Renewable energy

## 1 Introduction

Due to rising global electrical energy concerns, concepts of climate change, energy mix, renewable resources, reducing carbon emissions, and renewable-based microgrids have become hot topics of research. In this context, the grid-connected solar photovoltaic systems (SPVS) have gained more popularity over the decade in achieving low-carbon energy and electrifying the loads in remote areas[1,2]. However, the power systems at the point of common coupling (PCC) have been experiencing by the increasing penetration of renewable energy sources, the operational dynamics brought about by V2G and G2V concepts, and semiconductor loads, which have introduced power quality issues, variability, and uncertainty[3,4]. As a consequence, this scenario poses a challenge in terms of power quality issues and other grid-supported objectives in modern-day power systems, as depicted in Fig. 1. In this scenario, power electronic converters, (PECs) and their control systems play a crucial role, capable of addressing a wide range of objectives, as presented in Fig. 1. Generally, in a single-phase utility system, an H-bridge voltage source inverter (VSI) is endowed with a control system to integrate the renewable resources. Owing to the objectives, appreciable research has been conducted and published. Researchers consistently improve control systems to meet varied objectives. In a grid-connected applications, the PEC control system typically involves a reference estimation unit and a controller to track the reference.

Most reference estimation approaches are implemented using either the time or frequency domain and soft-computing techniques. Indeed, existing literature reports enhanced variants that

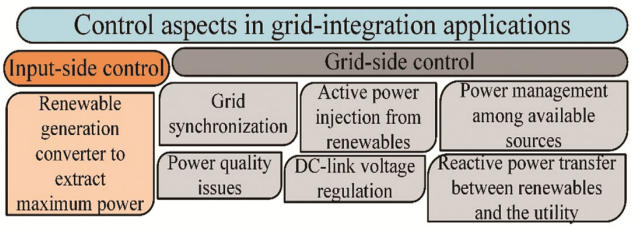


Fig. 1 — Control objectives

*Corresponding author: E-mail: tirumalasetty.chiranjeevi@smvdu.ac.in

incorporate data-adaptive techniques, state observers, as well as Kalman filters[5]. Although these methods can successfully estimate the reference signal for the grid-integrated VSI, they are not suitable for all operational conditions. These entail considerable computational complexity, particularly in the case of a frequency-domain techniques[6]. The approaches that are adaptable to data, such as machine learning and fuzzy-based algorithms, demonstrate effectiveness in delivering grid-supported features via the implementation of VSI[7]. Despite this, determining the optimal weighted gains and mapping functions poses significant challenges.

Recent studies prove a transition among researchers with the utilization of advanced hybrid algorithms for reference estimation, use of data-adaptive strategies[8-10]. Empirical mode decomposition (EMD) is a widely utilized way for decomposing non-stationary contaminated signals into intrinsic mode functions[11]. EMD's implementation faces challenges due to a mode-mixing issue influencing the compensation system. To address this issue, ensemble empirical mode decomposition (EEMD) has been recently introduced as an improvement over traditional EMD. Furthermore, alternative versions including CEEMD, CEEMDAN, and ICEEMDAN have been proposed[12]. The Adaptive Linear Neuron (Adaline) serves as a viable data-driven approach, demonstrating effectiveness in various complex domains, particularly in addressing voltage or current harmonics[13-16]. This represents a subclass of artificial neural networks (ANN). Adaline is designed to identify linear correlations between input signals and the desired outcome. This is a single-layer neural network defined by a linear activation function and a learning rule based on the least-mean-square (LMS) method[17]. Adaline-based fundamental extraction streamlines controller design and addresses several challenges associated with traditional methods. It provides the advantages of selective harmonic compensation. Further, the adaptability of the Adaline algorithm stems directly from its learning rule. It allows Adaline to function as a powerful and efficient adaptive filter that learns from data in real-time. It doesn't require complex mathematical models of the system; it simply learns by observing an error signal. Hence, simplifies the controller design by diminishing dependence on intricate filtering or transformation techniques.

Once the required reference is estimated, reference tracking by the associated PEC, also crucial in the grid-integrated SPVS applications. Usually, in conventional control systems, this objective is accomplished by a number of PI controllers in outer voltage and inner current loops. However, in this context, researchers have also developed nonlinear control[18] concepts for this purpose, and among them, the model predictive controller (MPC) has been used widely in grid- integrated applications[19-21]. In essence, MPC provides optimal gate drive signals for the PECs by considering the nonlinear switching dynamics of the same. Recent reviews highlight the transition to data-driven and AI-enhanced control strategies in contemporary power systems, especially regarding renewable integration and grid stability[22-25]. The proposed method leverages this momentum by providing a computationally efficient, adaptive framework that streamlines controller design while ensuring robustness in stochastic operating conditions.

Thus, inspiring from the literature, it is seen that the AI/ML-based algorithms are now considered the prior choice and are still a hot topic of research in grid-connected solar applications. Hence, this paper studied an Adaline algorithm that extracts the fundamental from the harmonically distorted currents. Moreover, the key facets of this research are highlighted as follows:

An Adaline algorithm is formulated for fundamental current estimation from harmonic distorted currents.

i The H-bridge VSI effectively provides the grid-supported ancillary features, besides the injection of SPVS-generated active power into the AC side.

ii The converters in the system are optimally controlled using a nonlinear current tracking controller, MPC.

iii Under stochastic operational scenarios, the common DC-link is regulated.

iv The source current total harmonic distortion (THD) is found quite satisfactory, thus satisfying the IEEE 1547-2018 standards.

Several research papers have examined data-adaptive techniques applied in grid-integrated applications; however, to the authors' knowledge, the application of Adaline control with MPC has not been explored or implemented under stochastic dynamic scenarios.

### 1.1 System Schematic of Grid-Integrated SPVS

he schematic arrangement of a grid-integrated SPVS through H-bridge VSI is shown in Fig. 2. All

T the utility- connected loads are powered from a power system via a circuit breaker (C.B.), under normal operational conditions. As depicted, the voltage and current of the utility system with line impedance ($r_s$, $L_s$) are represented as $v_s$ and $i_s$, respectively. The SPVS comprises a PV array with 9-series-connected modules per string, connected to the common DC link through a DC-DC boost converter. The filter parameters of the SPVS are represented as $r_p$ and $L_p$, as shown. The voltage across and the current from the PV array are $v_p$ and $i_p$, respectively. The DC-link capacitance is denoted as $C_{dc}$. The heart of the grid-integrated SPVS is the H-bridge VSI. It is connected in parallel with the utility system at the PCC and provides the grid-supported ancillary features, including the injection of generated active power from the SPVS. As shown, the H-bridge VSI has been equipped with 4 switches ($S_{u1}$,$S_{u2}$,$S_{b1}$,$S_{b2}$), and is operated in an opposite mode in each leg to avoid short-circuiting the common DC link voltage $V_{dc}$. The output current ($i_f$) of the VSI is filtered using $r_f$ and $L_f$ from the switching ripples. The voltage of the VSI is denoted as $v_f$. The voltage at the PCC is represented as $v_{pcc}$.

On the AC side, a nonlinear (diode-bridge rectifier) and linear loads are considered for the assessment. Similarly, on the DC side, local DC loads ($r_{d1}$ and $r_{d2}$) are considered with switch $s_d$ for the analysis. Nonetheless, besides the source variation (by solar irradiance), the switches $s_l$ and $s_d$ are considered to replicate the real-time load variation scenarios on the AC and DC sides, respectively.

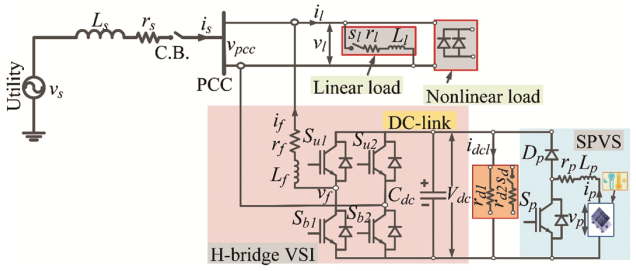


Fig. 2 — System Schematic of Grid-Integrated SPVS

## 2 Materials and methods

### 2.1 Control Strategy of Grid-Integrated SPVS

The control strategy encompasses estimating a required reference current, followed by a reference current tracking controller. The grid-integrated SPVS realizes multiple tasks, such as synchronizing issues, harnessing maximum power via the maximum-power point tracking (MPPT) algorithm, as well as injection of available SPVS active power into the utility, such that the power factor at the PCC remains at unity, and compensation of source current harmonics, and voltage regulation at the common DC-link. The above-mentioned specific control objectives are realized in this section for the grid-integrated SPVS. In this context, the mathematical and logical concepts for formulating an Adaline-based control strategy are illustrated in Figs. 2-3.

#### *2.1.1 Generation of Source Current Reference*

In general, the nonlinear load current ($i_l$) is composed of the fundamental component (50 *Hz*) and unwanted harmonic components. Thus, $i_l$ can be represented mathematically as follows:

$$i_l(t) = I_1 sin(n\omega_1 t + \varphi_n) \quad \ldots (1)$$

The above equation shows that il has two parts: instantaneous fundamental and harmonic mixing components. The load should only draw the utility grid or available PV's instantaneous fundamental power for effective power system operation. However, an external source (a grid-integrated inverter with a DC-link capacitor in this research) should also compensate for the load's necessary harmonic component. The source current fundamental must be extracted to implement indirect current control.

The Adaline estimator is used to estimate the fundamental load current $i_{lf}$ from a harmonic current, trained on a nominal sinusoidal current ($i^*$). The output ($i_{lf}$) of the Adaline is used to estimate the requisite source current reference ($i_{sr}$) using the reference estimation unit, as shown in Fig. 4. Similarly, the fundamental voltage required for sine

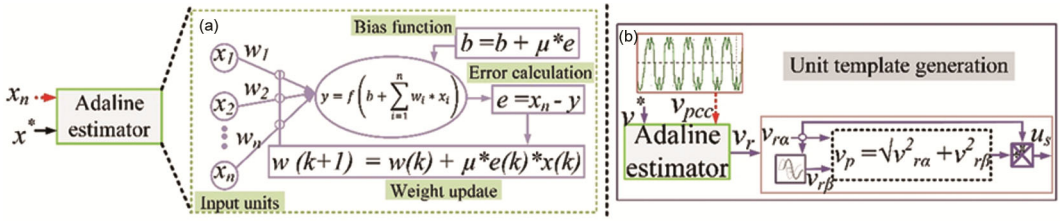


Fig. 3 — (a) Adaline Estimator; and (b) In-phase unit template

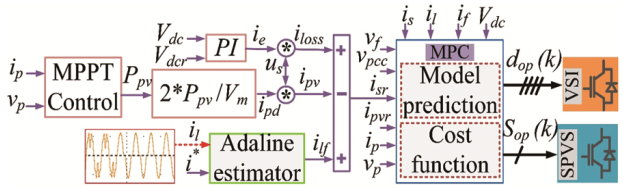


Fig. 4 — Control Strategy of Grid-Integrated SPVS

unit ($u_s$) template generation[26] is also extracted using the Adaline estimator, as depicted in Fig. 3 (b). Furthermore, the $i_{sr}$ is utilized for generating the optimal gate drive signal for the VSI using the MPC algorithm. The implementation of the Adaline estimator to estimate the $i_{lf}$ is presented below.

Adaline is a form of artificial neuron that adjusts its weights using the LMS algorithm. It is a linear model that modifies its parameters to minimize the discrepancy between predicted and actual values, making it suitable for a wide range of signal processing tasks. Fig. 3 (a) depicts a typical implementation scheme of the Adaline technique. As seen, a harmonic current/voltage ($= x_n$) and required current/voltage ($= x^*$) are applied as inputs of the Adaline estimator. The Adaline algorithm extracts the required fundamental $i_{lf}$ or $v_r$ (in case of distorted voltage) from a harmonic load current $i_l$. Here is an outline of how to implement the Adaline algorithm in the MATLAB/Simulink platform using an *Adaline.m* file:

i *Initialization:* Set the parameters, which include sampling frequency, learning rate ($\mu$), number of iterations (epoch), weights ($w$), bias ($b$), and fundamental frequency ($f_s$). The Adaline model for a specified input $i_l$ is expressed as follows:

$$i_{lf} = f(b + \sum_{i=1}^{n} w_i * i_i) \quad \ldots (2)$$

The bias term is responsible for adjustments related to the DC offset present in the signal.

ii *Iteration and convergence:* The Adaline algorithm operates by continuously adjusting the weights and bias through a learning rule, utilizing either the LMS algorithm or the Delta rule. This iterative process reduces the mean square error between the predicted output $i_{lf}$ and the nominal reference $i*$. The anticipated parameters for w and b are outlined as follows:

$$w(k+1) = w(k) + \mu * e(k) * i_l(k) \quad \ldots (3)$$

$$b(k+1) = b(k) + \mu * e(k) \quad \ldots (4)$$

error term $e(k)$ is the difference between the harmonized $i_l$ and the predicted output $i_{lf}$.

iii *Extracted fundamental:* After Adaline network training, the model learns $w$ and $b$ to optimally match the $i^*$ to the fundamental component of the harmonized $i_l$. The retrieved fundamental signal is rebuilt using learning weights and bias:

$$i_{fl} = f(b + w * i^*) \quad \ldots (5)$$

The Adaline essentially functions as an LPF, which emphasizes the 50 *Hz* and attenuates the undesired components. Once the fundamental component is obtained, then the requisite source current ($i_{sr}$) to be drawn from the utility is derived. In this framework, the loss component ($i_{loss}$) subjected to the VSI switching action is obtained using a PI controller. Similarly, the SPVS feed-forward term $i_{pd}$ is derived as depicted in Fig. 4. Now, the obtained $i_{loss}$ and $i_{pd}$ are multiplied by the synchronizing signal $u_s$, as shown in Fig. 4. The outcome will then be refined to obtain the required instantaneous source current reference, denoted as $i_{sr}$.

Algorithm 1 − Pseudo code of Adaline

*Step 1*: Initialization: Set initial weights
$w_{sin}$ ← small random value
$w_{cos}$ ← small random value
Set learning rate $\mu$, and
y[n] = 0, e[n] = 0.
*Step 2:* Adaptive Learning Loop:
*For n = 1 to N do*
→Generate reference sinusoids
$x_1 = sin(\omega_0 * n)$
$x_2 = cos(\omega_0 * n)$
→Estimate the fundamental component
$y[n] = w_{sin} * x_1 + w_{cos} * x_2$
→instantaneous error
$e[n] = x[n] - y[n]$
→Update weights using LMS rule
$w_{sin} = w_{sin} + \mu * e[n] * x_1$
$w_{cos} = w_{cos} + \mu * e[n] * x_2$
End
*Step3*. Outputs:
*y[n]* → extracted fundamental component
*e[n]* → residual signal (contains harmonics and noise)
End

### 2.2 MPC-based Reference Tracking

The MPC primarily begins by identifying the essential circuit laws necessary for predicting the

performance of the converters[27]. This is succeeded by deriving the discrete dynamics by the forward Euler approximation.

A cost function is then defined according to the set objectives, enabling the generation of optimal switching signals for the system's converters. Fig. 4 illustrates the execution framework for the MPC concept.

#### *2.2.1 Predictive Dynamics of VSI*

The dynamics of the VSI are formulated utilizing fundamental Kirchhoff rules. The first-order differential equation for the VSI current $i_f$ about the switching function $d$ is stated as:

$$L_f \frac{di_f}{dt} = d * V_{dc} - r_f i_f - v_{pcc} \quad \ldots (6)$$

$d$ is reliant upon the switching states allowed by the VSI and operates in conjunction with the converter leg's function. So, it can be stated as follows:

$$d = \begin{cases} 1, & (S_{u1}: ON, S_{b2}: ON) \\ -1, & (S_{b1}: ON, S_{u2}: ON) \end{cases} \quad \ldots (7)$$

The system currents at the PCC can be stated as follows:

$$i_s + i_f = i_l \quad \ldots (8)$$

At the time instant $t = k + 1$, the forward-Euler approximation can be used to represent the predictive current $i_f(k+1)$ with a sampling time $T_s$, as shown below:

$$i_f(k+1) \approx i_f(k) + \frac{T_s}{L_f}\left[d * V_{dc}(k) - r_f i_f(k) - v_{pcc}(k)\right] \quad \ldots (9)$$

Similarly, Eq. (8) can be written as:

$$i_s(k+1) + i_f(k+1) \approx i_l(k+1) \quad \ldots (10)$$

The actual values of $v_{pcc}$ and $i_l$ can be considered constant during the subsequent two sampling scenarios, assuming a small value of $T_s = 10\ \mu sec$. It is to be noted that the chosen $T_s$ ensures sufficient resolution for dynamic tracking while maintaining computational feasibility and found to be within acceptable bounds for real-time operation (using OPAL-RT OP4512) under the verified conditions. The subsequent equations can be derived in the following manner.

$$v_{pcc}(k+1) \approx v_{pcc}(k) \quad \ldots (11)$$

$$i_l(k+1) \approx i_l(k) \quad \ldots (12)$$

#### *2.2.2 Predictive Dynamics of SPVS Converter*

The DC-DC boost converter of the SPVS is responsible for operating the MPPT under dynamic irradiance levels.

The dynamics for the SPVS converter with a switching function $S_{pv}$ are stated as follows:

$$\frac{di_{pv}}{dt} = \frac{V_{pv}}{L_{pv}} - \frac{r_{pv} i_{pv}}{L_{pv}} - [1-d] * \frac{V_{dc}}{L_{pv}} \quad \ldots (13)$$

where $d$ is dependent on the converter switching states (1 or 0), and it can be stated as:

$$d = \begin{cases} 0\ for\ OFF\ position\ of\ the\ S_{pv} \\ 1\ for\ ON\ position\ of\ the\ S_{pv} \end{cases} \quad \ldots (14)$$

Algorithm 2 − MPC pseudo code of VSI

*Step 1*: At the $k^{th}$ instant, sense the required currents & voltages.

*Step 2*: Initialize: $n_s \leftarrow 0$, $(d) \leftarrow 0$, $g_{sopt} \leftarrow \infty$.

*Step 3*: Increase counter $n_s \leftarrow n_s + 1$.

*Step 4*: Predict: $i_s \rightarrow (d)$ at $k+1$ instant using Eq. (9).

*Step 5*: Retrieve $i_{sr}$ from the reference source current.

*Step 6*: Determine the cost function $g_s$.

*Step 7*: Check *if* $g_s < g_{sopt}$ then $g_{sopt} \leftarrow g_s$.

*Step 8*: Check *if* $n_s < 4$ go to step-3, *else* $g_{opt}$ = *min.*[ $g_s$ $(n_s)$]; and apply $d$ correspond to *min.*[ $g_s$ $(n_s)$].

The predictive current $i_{pv}(k+1)$ can be stated as:

$$i_{pv}(k+1) \approx i_{pv}(k) + \frac{T_s}{L_{pv}}\left[V_{pv}(k) - r_{pv} i_{pv}(k) - [1-d] * V_{dc}(k)\right] \quad \ldots (15)$$

Now, the cost functions are defined using the objectives of the VSI and SPVS converters, as follows[28]:

$$g_s = (i_{sr} - i_s(k+1))^2 \quad \ldots (16)$$

$$g_{sp} = \left(i_{pvr} - i_{pv}(k+1)\right)^2 \quad \ldots (17)$$

where $g_s$ and $g_{sp}$ represent the cost functions of the MFHC and PV converter, respectively. Substituting $i_{sr}(k)$, generated from the reference

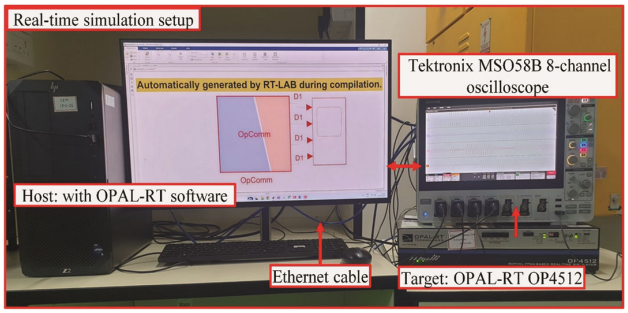


Fig. 5 — OPAL-RT OP4512 setup

Table 1 — System parameters

| Parameter | Numerical Value |
|---|---|
| $v_{pcc}, f_s$ | 230 $V$, 50 $Hz$ |
| $r_s, L_s$ | 0.02 Ω, 0.2 $mH$ |
| $r_f, L_f$ | 0.2 Ω, 50 $mH$ |
| $C_{dc}, V_{dc}$ | 4000 $\mu$F, 400 $V$ |
| $r_1, r_2, L_l, C$ | 25 Ω, 75 Ω, 10 mH, 3900 µF |
| $r_{d1}, r_{d2}$ | 250 Ω, 650 Ω |
| DBR | 42.5 Ω, 10 $mH$, 3900 $\mu$F |

estimation unit, into Eq. (16) yields a series of values ($g_1$, $g_2$, $g_3$, $g_4$), identifying the minimal value $g_{s,min.}$. To minimize the error between isr and $i_s(k+1)$, the optimal control switching action is $S_{op}$. In MATLAB/Simulink implementation, the MPC approach is written as an S-Function with pseudocode given in Algorithm 2. Similar steps are taken for the SPVS converter, considering ($i_{pvr} = i_{mpp}$) with two possible switching states in Eq. (14) to generate the optimal switching signal $d_{op}$.

## 3 Results and Discussion

The Adaline-based MPC technique was evaluated using MATLAB/Simulink and a real-time simulator, the OPAL-RT OP4512, shown in Fig. 5. The grid-integrated SPVS along with the proposed control system is modeled first developed in the MATLAB/Simulink platform. The developed model is then separated into the master and console subsystems using relevant communication blocks for instance Analog in, Analog out, Opctrl, and Opcom. The host device (PC) and the target device (OP4512) communicate via an Ethernet wire using TCP/IP. Next, a USB drive retrieves the results via the Tektronix MDO4000, $500M\ Hz$, $2.5GS/s$ oscilloscope's USB ports. The real-time simulator, OP4512 is equipped with an Intel® Xeon® E3 quad-core processor (3.7 GHz) and a Xilinx® Kintex-7 410T FPGA board. The system was configured with a sampling frequency of 100 kHz ($T_s = 10\mu sec.$) to ensure high-fidelity signal tracking and control responsiveness. Refer to Table 1 for system configuration parameters. The diode bridge rectifier (DBR) is taken as a nonlinear load ($r$, $L$, $C$ are connected in a T-section at the output of DBR). Moreover, average daily local data at a standard temperature of $27^0C$ is used to analyze solar irradiance variation from 148 to 860 $W/m^2$.

To evaluate the feasibility of the proposed control system in response to realistic, and unpredictable occurrences, the stochastic variations in solar irradiance were simulated using a signal builder block from the MATLAB/Simulink in-built library. A voltage distortion from 0.2 to 0.3 seconds is considered at the source voltage $v_{pcc}$. Such that, then mathematically $v_{pcc}$ is expressed as: It is superimposed with 3rd and 7th order harmonics, such that, the expression for resultant $v_{pcc}$ is given as:

$$v_{pcc} = 230sin\ 2\pi * f_s + 76.66\ sin\ 2\pi * 3 * fs + 32.85 * sin\ 2\pi * 7 * fs \quad \ldots (18)$$

### 3.1 GSM-1 (0−0.35 sec):

During this operating mode, the irradiance is considered as 148 $W/m^2$ (0−0.25) and 452 $W/m^2$ (0.25−0.35). As shown in Figs. 6-7 the $i_s$ is observed as sinusoidal and harmonic-free, irrespective of nonlinear $i_l$ with harmonics. In this scenario, the H-bridge VSI current $i_f$ injects the available solar PV current into the utility from the SPVS, thereby supporting the compensation of load harmonics as well. During this operation mode, $v_{pcc}$ and $i_s$ are in-phase.

Besides the harmonics present in $v_{pcc}$ during 0.2−0.3 seconds, the $i_s$ is observed as sinusoidal with improved THD.

### 3.2 GIM (0.35−0.5 sec):

During the GIM operation, it is assumed that the maximum power is available from the SPVS and is fed into the utility to support the total load demand. In this scenario, the irradiance is maintained at 860 $W/m^2$ from 0.35−0.6 seconds. From the obtained results, it is observed that apart from maintaining UPF, the phase relation between $v_{pcc}$ and $i_s$ is out-of-phase. Hence, this mode of operation is known as the grid-injection mode.

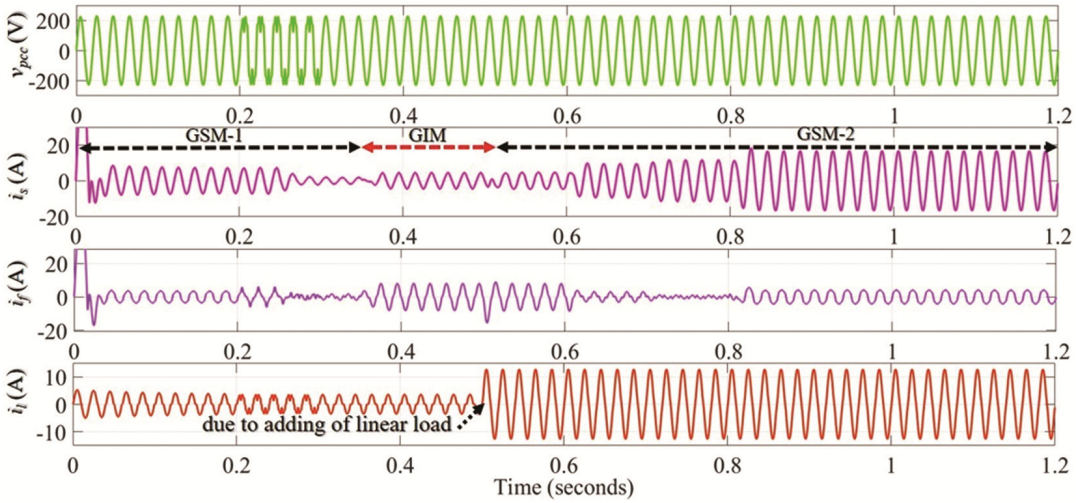


Fig. 6 — Simulated results under dynamic operation

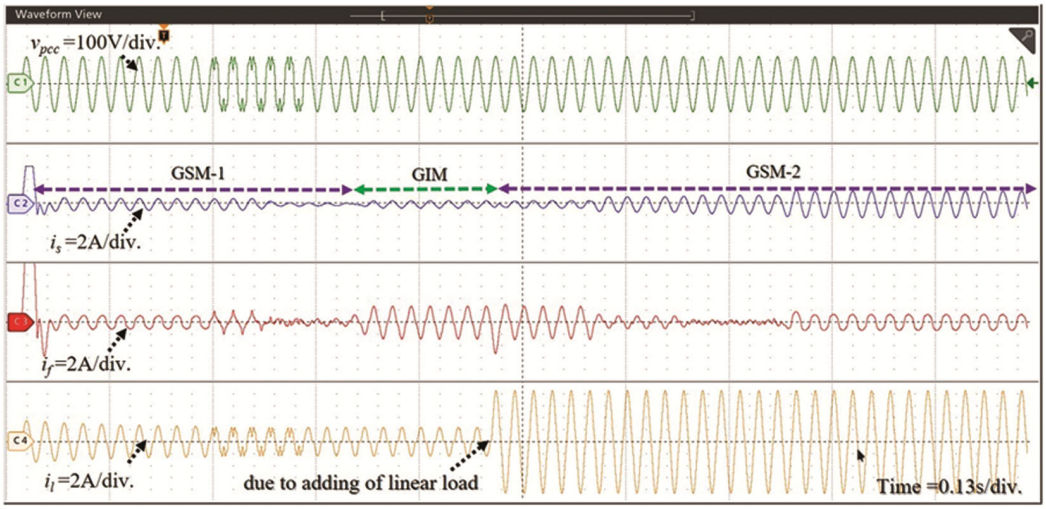


Fig. 7 — OPAL-RT OP4512 results under dynamic operation

In this scenario, besides the harmonic current compensation, the H-bridge VSI current $i_f$ injects the excess available solar PV current into the utility from the SPVS.

**3.3 GSM-2 (0.5−1.2 sec):**

In the GSM-2 operation scenario, illustrated in Fig. 6, a linear load is connected at the PCC at t = 0.5 seconds. A DC load of 650 $\Omega$ is connected to the common DC-link at t = 0.7 seconds. The irradiance varies from 860 $W/m^2$to 534 $W/m^2$ between 0.6 and 0.8 seconds, subsequently decreasing to 234 $W/m^2$ from 0.8 to 1.2 seconds. In this scenario, the system meets the additional load demand using the available solar power via the VSI, while the utility source provides support for the deficit power. It is noted that, similar to GSM-1, the $v_{pcc}$ and $i_s$ exhibit in-phase characteristics.

Figure 8 illustrates the system DC parameters ($i_{dcl}$, $i_{pv}$, and $V_{dc}$) response during a dynamic scenario. Further, the results corresponding to the OPAL-RT OP4512 are presented in Fig. 9. The current $i_{pv}$ is shown to vary following changes in irradiance, facilitated by the MPPT algorithm. The DC-link voltage $V_{dc}$ is consistently maintained at the reference value of 400 $V$, $V_{dcref}$, across all dynamic conditions. This demonstrates the impact, control flexibility, and efficacy of the Adaline-based MPC approach applied to grid-integrated SPVS. Figure 10 illustrates the power management in Watts among available SPVS ($P_{pv}$), utility source ($P_{sl}$), injecting by VSI ($P_f$), utility-connected load ($P_l$), and DC load

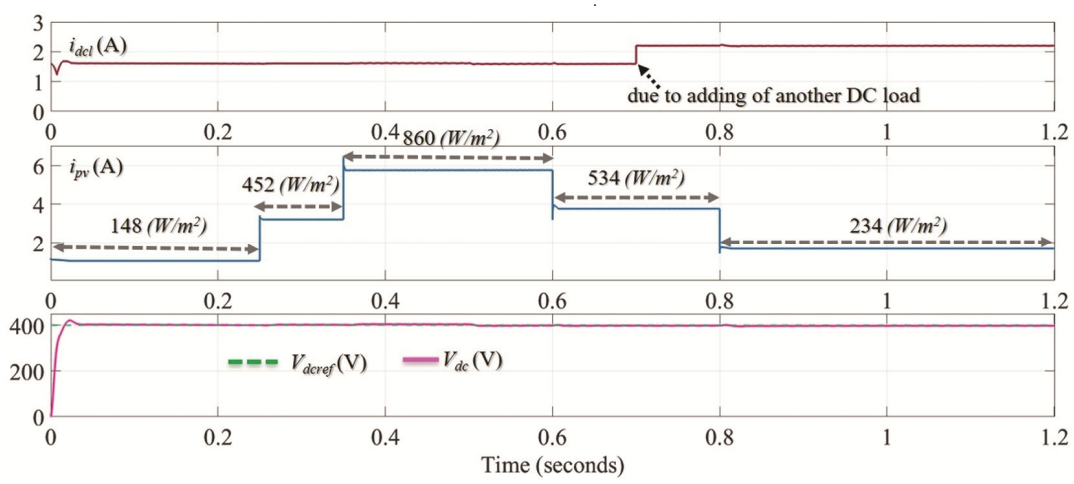


Fig. 8 — Simulated results for DC parameters

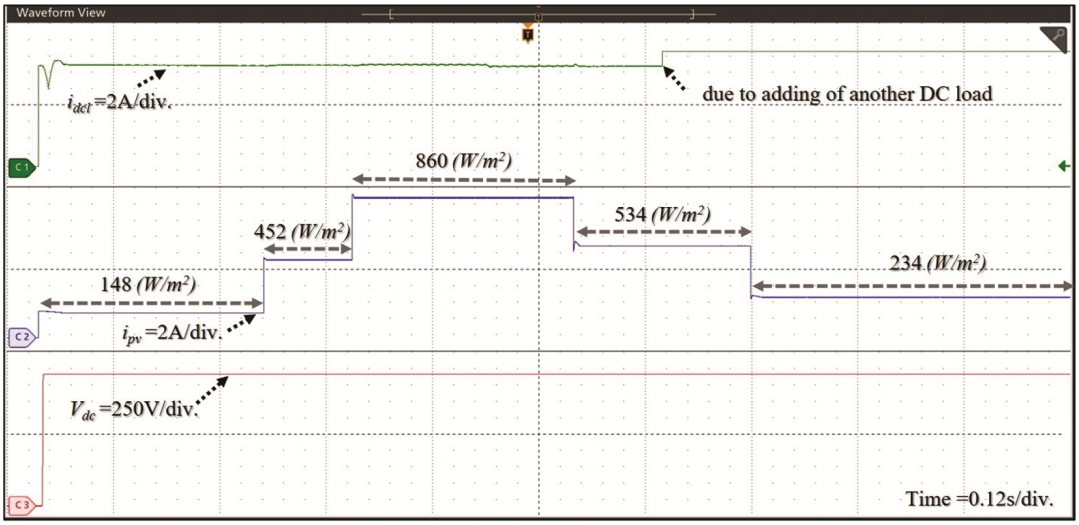


Fig. 9 — Simulated results for DC parameters

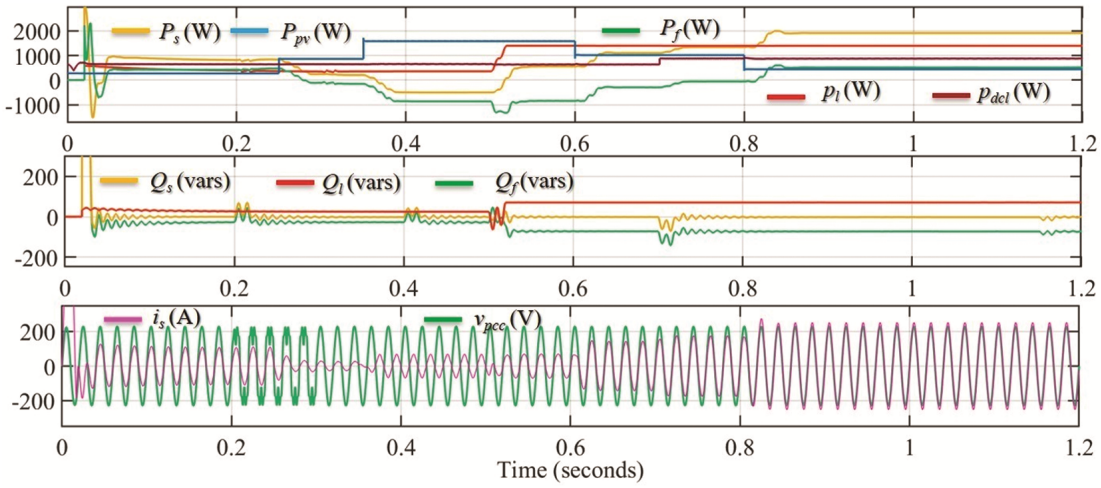


Fig. 10 — Power management under dynamic operation

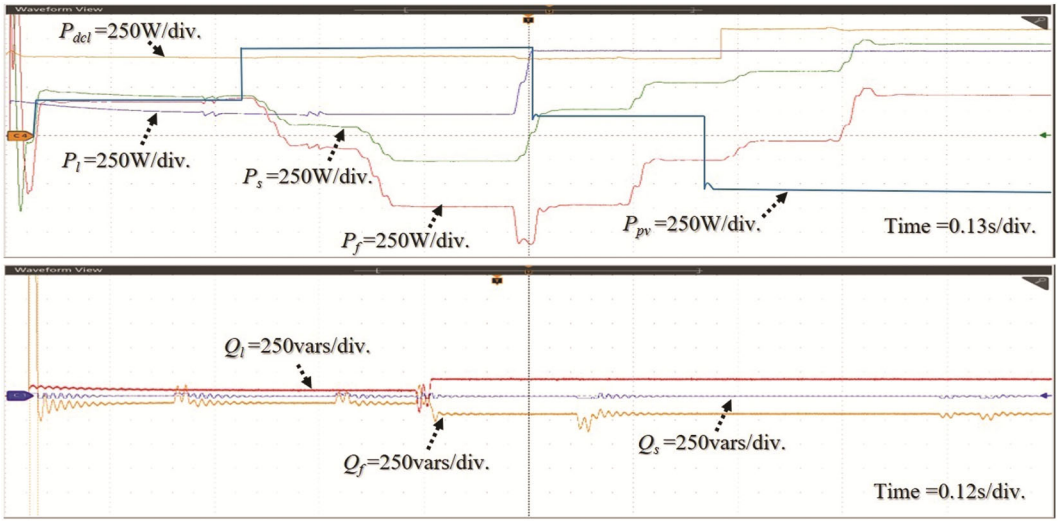


Fig. 11 — OPAL-RT-based results for power management

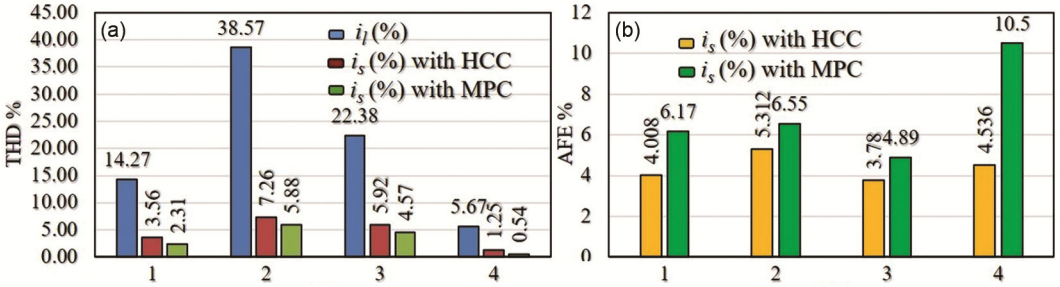


Fig. 12 — Performance evaluation

($P_{dcl}$), followed by the reactive power in vars of the load ($Q_l$), VSI ($Q_f$ ) and utility system ($Q_s$).

The supported power management results with OPAL-RT OP4512 are presented in Fig. 11. As seen, due to the indirect current control approach, the SPVS-supported VSI supports the load reactive vars, such that no reactive vars are drawn from the utility source. Moreover, the results (in Fig. 10) also illustrate the relation of $v_{pcc}$ and $i_s$ under different operating modes. For analysis purposes, $i_s$ is multiplied by a gain of 15 to its actual sensed value. During GSM-1 and GSM-2, it is noted that $v_{pcc}$ and $i_s$ exhibit in-phase behavior, whereas they are out-of-phase during GIM. It is observed that the power factor before compensation is 0.881, while after compensation it is 0.909.

In addition to the presented results above, the performance metrics such as THD and active filtering efficiency (AFE) are also assessed under considered dynamic operational scenarios. MATLAB/Simulink's FFT window provides the THD data for four simulated operation time scales.

Table 2 — THD analysis

| GSM-1 | | GIM | | GSM-2 | |
|---|---|---|---|---|---|
| HCC | MPC | HCC | MPC | HCC | MPC |
| $i_s$ | $i_s$ | $i_s$ | $i_s$ | $i_s$ | $i_s$ |
| 3.56 | 2.31 | 5.92 | 4.57 | 1.25 | 0.54 |

Figure 12 (a) demonstrates the THD analysis with the conventional controller, based on the hysteresis current controller (HCC) and MPC as well. The same numerical are presented in Table 2. As shown in Fig. 12 (a), THD analysis is a measure for 4-cycles at t = 0.05, 0.2, 0.4, and 0.6, as 1, 2, 3, and 4, respectively. It is observed that, in all operating modes, the Adaline-MPC approach provides improved THD in source current $i_s$, even though high THD content is present in the current drawn by the load connected at PCC. These results complying with the IEEE 1547-2018 standard[29] for THD limits in grid-integrated applications. To keep the power quality and security of the grid, IEEE 1547-2018 states that distributed energy resources (DERs) must follow the harmonic limits set by

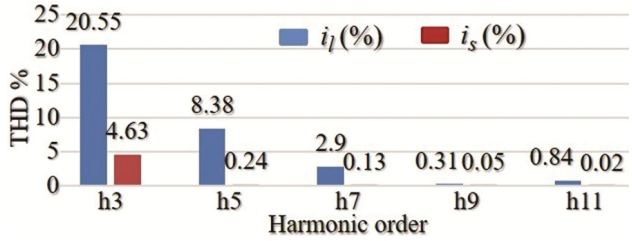


Fig. 13 — Harmonic orders

IEEE Std 519. All DERs—such as solar inverters, energy storage systems, and other devices that are connected to the grid—must limit the amount of harmonic current that flows into the PCC. Harmonic orders (e.g., 3rd, 5th, 7th, etc.) have individual current distortion limits, typically ranging from 2.5% to 4% depending on the harmonic order and system characteristics. As shown in Fig. 13, THD analysis is a measure for 7-cycles at t = 0.35, during GIM. It is observed that, all harmonic orders (up to 11th), the Adeline-MPC approach provides improved THD and satisfies the IEEE 1547-2018 standard requirements in source current $i_s$, in contrast to the high THD content $i_l$, as presented. Besides, the THD numerical obtained during GSM-1, GIM, and GSM-2 with HCC, and MPC are presented in the Table 2. It is observed that the THD of $i_l$ during GSM-1, GIM, and GSM-2 are 14.27%, 22.38%, and 5.67, respectively. Additionally, the assessment of AFE, characterized[2] as the ratio of $i_{lrms}$ to $i_{srms}$ expressed in percentage, is illustrated in Fig. 12 (b). According to the definition of AFE, $i_{srms}$ exhibits an inverse proportionality to itself. As the source current harmonics decrease, the value of $i_{srms}$ also diminishes, leading to an increased AFE, and conversely. Figure 12 clearly shows that the Adaline-MPC exhibits a superior AFE when compared to the Adaline HCC. As a result, it is evident that the Adaline-MPC-controlled VSI demonstrates notable performance, underscoring enhanced adaptation for flexible control in grid-connected applications. It is to be noted that, based on the MATLAB/Simulink reporting and benchmarking on a representative low-cost DSP (e.g., TI F28379D), the average computation time per cycle can found to be approximately 09–11μ sec., which remains comfortably within the 10μ sec. sampling interval used in this study. This confirms the suitability of the proposed method for real-time implementation on resource-constrained embedded platforms.

## 4 Conclusion

This study implements a control strategy based on Adaline-MPC for applications involving grid-integrated SPVS. The SPVS benefits from the utility connection in the absence of solar irradiance and does not need any battery storage. The Adaline algorithm is capable of estimating the fundamental component necessary to determine reference utility source currents from harmonically distorted load currents. The MPC provides the optimal gate drive signals for the system converters, comprising the VSI and the boost converter. The assessed control strategy enables the transition between different operating modes, thus improving power balance with the utility grid and supporting the integration of solar photovoltaic energy. The total load demand is satisfied by the readily available solar energy via grid-integrated VSI, with the utility grid supplying compensation for any shortfalls. The topological structure of the H-bridge VSI enables it to support connected DC loads when there is a lack or deficiency of power from the SPVS. Further, the common DC-link voltage is regulated and maintained at the nominal reference 400 V. Despite an increase in load current THD, the THD of the source current improves across different operating modes, thereby complying with the IEEE 1547-2018 standard. Besides, the AFE is enhanced with the support of Adaline-MPC in contrast to the conventional HCC.

Future studies will involve the extraction of features related to adverse real-time events in poly-phase systems, including current and voltage quality concerns in modern power systems that incorporate renewables in microgrids. Hardware testing of the Adaline-MPC may be necessary to meet the grid-integration objectives. Future research should employ on- line Adaline estimate implementation with real-time data and optimal parameter selection, rather than utilizing pre-recorded harmonically distorted data. The hybrid control approach should be enhanced to determine the requisite current/voltage reference signals for grid-forming converters intended for future use with energy storage devices.

## References

1 Priyadarshi N, Padmanaban S, Holm-Nielsen J B, Blaabjerg F & Bhaskar M S, *IEEE Syst J,* 14 (1) (2019) 1218.

2 Majji R K, Mishra J P & Dongre A A, *Int J Emerg Electr Power Syst,* 23 (5) (2022) 715.

3 Majji R K, Chiranjeevi T, *et al*, *AEU-Int J Electron Commun,* 187 (2024) 155560.
4 Singh S K, Agarwal A & Kanumuri T, *Ind J Pure & Appl Phys (IJPAP)*, 60 (9) (2022) 754.
5 Bushra E, Zeb K, Ahmad I & Khalid M, *Result Eng,* 22 (2024) 102213.
6 Godoy Simo˜es M, Harirchi F, Babakmehr M, *IET Smart Grid*, 2 (4) (2019) 491.
7 Popescu M, Bitoleanu A, Suru C V, Linca M & Alboteanu L, *Energies*, 17 (12) (2024) 2867.
8 Alqaraghuli S M & Karan O, *Babylonian J Artificial Intelligence*, 2024 (2024) 34.
9 Samanta I S, Mohanty S, Parida S M, Rout P K, Panda S, Bajaj M, Blazek V, Prokop L & Misak S, *Result Eng*, 25 (2024) 103873.
10 Venugopal G, Udayakumar A K, Saha N, Kalavathy A N, Balashanmugham A & Vasudevan B, *Comp Electr Eng*, 111 (2023) 108952.
11 Park J, Pao G M, Sugihara G, Stabenau E & Lorimer T, Empirical mode modeling: *Nonlinear Dynamic,* 108 (3) (2022) 2147.
12 Shihabudheen K, Gupta S, *et al*, *Comp Electr Eng*, 109 (2023) 108770.
13 Singh B, Jayaprakash P & Kothari D, *J Power Electron*, 9 (3) (2009) 386.
14 Rai R K & Sinha U K, *Ind J Pure & Appl Phys (IJPAP)*, 63 (8) (2025) 719.
15 Babes B, Latre`che S, Bouafassa A, Aissa O, Badoud A E, Khemliche M, Bajaj M & Zaitsev I, *Sci Rep*, 14 (1) (2024) 12775.
16 Irfan M M, Alharbi M & Basha C H, *Sci Rep*, 15 (1) (2025) 5016.
17 Han Y, Xu L, Khan M M, Chen C, Yao G & Zhou L-D, *IEEE Trans industrial electr*, 58 (9) (2010) 3893.
18 Kumar R & Bansal H O, *Sustain Cities Soc,* 42 (2018) 574.
19 Vazquez S, Rodriguez J, Rivera M, Franquelo L G & Norambuena M, *IEEE Trans Industrial Electron,* 64 (2) (2016) 935.
20 Majji R K, Mishra J P & Dongre A A, *Sustain Energy Technol Assess,* 54 (2022) 102862.
21 Majji R K, Mishra J P & Dongre A A, *Arabian J Sci Eng,* 48 (2023) 14845.
22 Babayomi Oluleke, *et al*, "Advanced control of grid-connected microgrids: challenges, advances and trends" *IEEE Trans Power Electron*, 40 (2025) 7681.
23 Bertozzi Otavio, *et al*, *IET Energy Syst Integr*, 6 (3) (2024) 197.
24 Subedi S, Gui Y & Xue Y, *IEEE Trans Industry Appl*, 61 (2025) 2434.
25 Huang Y, Huo S & Dong Y, *Int J Gen Syst*, in press, (2025) 1.
26 Jain C & Singh B, *IET Gener, Trans Distribut*, 9 (10) (2015) 886.
27 Majji R K, Mishra J P & Dongre A A, 3rd *International Conference on Energy, Power and Environment: Towards Clean Energy Technologies IEEE*, 2021 p. 1.
28 Majji R K, Mishra J P & Dongre A A, *IETE J Res*, 70 (2023) 1.
29 Johnson J, Fox B, Kaur K & Anandan J, *IEEE Access*, 9 (2021) 142129.